Searching for DFT-based methods that include dispersion interactions to calculate the physisorption of H$_2$ on benzene and graphene

I. Cabria, M. J. López, and J. A. Alonso

Articles you may be interested in

Communication: Density functional theory embedding with the orthogonality constrained basis set expansion procedure
The Journal of Chemical Physics **146**, 211101 (2017); 10.1063/1.4984777

Long-range interactions from the many-pair expansion: A different avenue to dispersion in DFT
The Journal of Chemical Physics **146**, 024111 (2017); 10.1063/1.4973728

Perspective: Found in translation: Quantum chemical tools for grasping non-covalent interactions
The Journal of Chemical Physics **146**, 120901 (2017); 10.1063/1.4978951

Low scaling random-phase approximation electron correlation method including exchange interactions using localised orbitals
The Journal of Chemical Physics **146**, 174110 (2017); 10.1063/1.4981817

On the physical interpretation of the nuclear molecular orbital energy
The Journal of Chemical Physics **146**, 214103 (2017); 10.1063/1.4984098

Announcement: Top reviewers for The Journal of Chemical Physics 2016
The Journal of Chemical Physics **146**, 100201 (2017); 10.1063/1.4978399

Searching for DFT-based methods that include dispersion interactions to calculate the physisorption of H_2 on benzene and graphene

I. Cabria, M. J. López, and J. A. Alonso
Departamento de Física Teórica, Atómica y Óptica, Universidad de Valladolid, 47011 Valladolid, Spain

Simulations of the hydrogen storage capacities of nanoporous carbons require an accurate treatment of the interaction of the hydrogen molecule with the graphite-like surfaces of the carbon pores, which is dominated by the dispersion forces. These interactions are described accurately by high level quantum chemistry methods, like the Coupled Cluster method with single and double excitations and a non-iterative correction for triple excitations (CCSD(T)), but those methods are computationally very expensive for large systems and for massive simulations. Density functional theory (DFT)-based methods that include dispersion interactions at different levels of complexity are less accurate, but computationally less expensive. In order to find DFT-methods that include dispersion interactions to calculate the physisorption of H_2 on benzene and graphene, with a reasonable compromise between accuracy and computational cost, CCSD(T), Møller-Plesset second-order perturbation theory method, and several DFT-methods have been used to calculate the interaction energy curves of H_2 on benzene and graphene. DFT calculations are compared with CCSD(T) calculations, in the case of H_2 on benzene, and with experimental data, in the case of H_2 on graphene. Among the DFT methods studied, the B97D, RVV10, and PBE+DCACP methods yield interaction energy curves of H_2-benzene in remarkable agreement with the interaction energy curve obtained with the CCSD(T) method. With regards to graphene, the rev-vdW-DF2, PBE-XDM, PBE-D2, and RVV10 methods yield adsorption energies of the lowest level of H_2 on graphene, very close to the experimental data. *Published by AIP Publishing.* [http://dx.doi.org/10.1063/1.4984106]

I. INTRODUCTION

Hydrogen is a candidate to replace gasoline in the cars of the future. Hydrogen can be stored in a solid material through different mechanisms: physisorption, chemisorption, and chemical reactions. Among the solid materials investigated, nanoporous carbons attract much attention because these are light materials and have large porosity, and consequently high specific surface areas available for hydrogen adsorption.[1–13] Nanoporous carbons store hydrogen through physisorption on the walls of the pores. Computer simulations have been performed to interpret the experimental results on hydrogen storage on nanoporous carbons and to make predictions for new carbon-based materials.[14–23] The theoretical calculations of the hydrogen storage capacities of these materials require an accurate description of the interaction energy curves of a H_2 molecule physisorbed on the carbon surfaces. The hydrogen storage capacity of nanoporous carbons depends not only on the region around the minimum of the interaction energy curve, but also on the shape of the interaction energy curve in the region far from the carbon surface, the tail region, especially in the case of wide pores.[19,21,22]

There are two sources of information on the interaction of H_2 with carbon-based surfaces: experiments and theoretical calculations. However, the reported experimental and theoretical results vary greatly. The measured adsorption energies of H_2 on carbon surfaces vary between 0.035 and 0.110 eV per H_2 molecule, because the structure of the carbon surfaces is

different. The results from theoretical calculations (adsorption energies, storage capacities, etc.) also vary greatly, depending on the model used to simulate the carbon-based surface and on the theoretical method. Hence, to clarify matters, one should study very specific carbon-based surface models using accurate theoretical methods.

The interaction of H_2 with a graphite-like carbon surface is a noncovalent interaction. Long range dispersion forces provide an important contribution to the interaction of H_2 with graphitic surfaces. The dispersion forces are weak, and they are difficult to include in the theoretical calculations. High-level *ab initio* methods such as the Coupled Cluster method with single and double excitations and a non-iterative correction for triple excitations (CCSD(T))[24] give a good account of the dispersion interactions. Møller-Plesset second-order perturbation theory method (MP2)[25] does not reproduce well screening effects and sometimes is affected by important errors also in small systems, like the benzene dimer. On the other hand, the local density approximation (LDA) and the generalized gradient approximation (GGA) versions of the density functional theory (DFT) do not include dispersion interactions. Nowadays, the best method to treat noncovalent interactions is CCSD(T).[26–28] Both CCSD(T) and MP2 methods are expected to yield accurate interaction energy curves for H_2 on a graphitic carbon surface, but these two methods are computationally expensive and are therefore restricted to small systems. The computational cost of the CCSD(T), MP2, and DFT methods scales as $O(N^7)$, $O(N^5)$, and $O(N^3)$, respectively, where N is proportional to the system size. Then, it would be desirable to

find DFT-based methods that include dispersion corrections and reproduce accurately the CCSD(T) interaction energy curve of H_2 on a carbon surface, with a compromise between accuracy and computational cost.

In the last fifteen years, DFT-based methods including dispersion interactions have been developed and tested in many dispersion-dominated systems. Klimeš and Michaelides[29] have reviewed the different DFT-based methods that include dispersion. One class of those DFT-based methods uses energy functionals that do not depend on external input parameters, and the dispersion interactions are obtained directly from the electron density. Those functionals are termed non-local correlation functionals because non-local correlations are added to local or semi-local correlation functionals. Among the methods based on non-local DFT functionals are the van der Waals Density Functional (vdW-DF) schemes[30–38] and the VV10[39] and RVV10 methods.[40]

A second class of DFT-based methods uses functionals which include the dispersion interactions empirically or semiempirically at different levels of complexity. Among those methods are the DFT-D schemes,[41] the DFT+DCACP method,[42–46] which is based on dispersion corrected atom centered pseudopotentials (DCACPs), the Tkatchenko-Scheffler (TS) method,[47] the exchange-hole dipole moment (XDM) method,[48,49] and the vdW/DFT-WF method,[50–54] which is based on maximally localized Wannier functions. DFT-D stands for Density Functional Theory with empirical Dispersion corrections. In the DFT-D scheme, an energy term is added, taking into account the dispersion interactions. That energy term includes some constants whose values are obtained empirically and remain constant throughout the calculation.

Dispersion can also be modelled by using effective atom-centered nonlocal pseudopotentials, such as the dispersion corrected atom centered pseudopotentials, DCACPs, developed by Rothlisberger and co-workers.[42–46] The parameters of these pseudopotentials were obtained by fitting the values of the properties of weakly bonded dimers of H_2, benzene, N_2, CO_2, He, Ne, Ar, and Kr[45,46] to the results of high-level *ab initio* calculations. The calculations are done with the unmodified density functional plus the corresponding DCACPs, and this is called the DFT+DCACP method. In the present work, we have performed PBE+DCACP calculations.

Comparisons of the binding energies, equilibrium geometries, and interaction energy curves of systems bonded by dispersion interactions, obtained with CCSD(T), MP2, DFT, DFT-D, and vdW-DF methods, have been published.[19,26,30,36,54–62] The interaction energy curve between H_2 and a carbon surface is a basic ingredient in the models developed to predict the hydrogen storage capacities of porous carbons.[17,18,21,63] Some previous publications compared the interaction energy curves of H_2 on benzene, graphene, and nanotubes. Mpourmpakis and Froudakis[19] have compared the interaction energy curves of H_2 with (6,6), (9,9), and (11,11) carbon nanotubes obtained with MP2 and DFT methods, modeling the nanotubes as $C_{24}H_{12}$ clusters with the curvature of the respective nanotubes. The DFT methods tested included LDA, GGA, and hybrid functionals, but dispersion interactions were not included. They also performed CCSD calculations,

but only at two separation distances. Costanzo *et al.*[52] compared the interaction energy curves of H_2 on graphene obtained with a DFT-D, a vdW-DF method, and the DFT/vdW-WF method.

There are studies and comparisons of H_2 physisorbed on benzene and graphene in the scientific literature, but as far as we know, those studies involve only some functionals that include dispersion interactions. There is a lack of a comparison of the interaction energy curves of H_2 on benzene and graphene obtained with CCSD(T) and with the main DFT-based methods that include dispersion interactions. The purpose of the present work is to make that comparison for the main and most popular DFT-based methods that include dispersion interactions, in order to evaluate their performance to describe the physisorption of molecular hydrogen on benzene and graphene.

Benzene is the simplest carbon-based surface, and graphene is one of the largest carbon-based surfaces. Benzene is a small molecule, and therefore it is feasible to make accurate CCSD(T) calculations of the interaction of H_2 on benzene. The H_2-benzene interaction energy curves obtained with DFT-based methods will be compared with the CCSD(T) interaction energy curve, the best theoretical curve. On the other hand, the DFT calculations of the H_2-graphene system will be compared with experimental data, in particular, with the experimental adsorption energy of the lowest level of H_2 physisorbed on graphene.[64]

In the present work, the results of CCSD(T),[24] MP2,[25] PBE,[65,66] VWN,[67] PW91,[68] PBE+DCACP,[42–45] B97D,[41,69] PBE-D2,[41] PBE-TS,[47] PBE-XDM,[48,49] vdW-DF,[30] optB88-vdW,[32] optB86b-vdW,[33] vdW-DF-cx,[34] vdW-DF-C09,[35] vdW-DF2,[36] vdW-DF2-C09,[37] rev-vdW-DF2,[38] and RVV10[40] calculations of H_2 physisorbed on benzene and the results of PBE, PBE+DCACP, PBE-D2, PBE-TS, PBE-XDM, vdW-DF, optB88-vdW, optB86b-vdW, vdW-DF-cx, vdW-DF-C09, vdW-DF2, vdW-DF2-C09, rev-vdW-DF2, and RVV10 calculations of H_2 physisorbed on graphene are presented. The calculations have been performed with three computational codes: Gaussian 09,[70] BigDFT,[71–73] and Quantum Espresso, QE.[74,75] In Sec. II, the computational codes and the parameters used are briefly presented. Section III consists of the discussion and comparison of the interaction energy curves of H_2 on benzene and graphene, obtained with all the methods. The conclusions are presented in Sec. IV.

II. COMPUTATIONAL METHODS

Three codes have been used to carry out the present calculations of H_2 on benzene and graphene: Gaussian 09 (G09), BigDFT, and Quantum Espresso (QE). DFT and DFT-based methods that include dispersion interactions are implemented in these codes. We have followed the same procedures with the three codes: For each of the methods used, the geometries of H_2, benzene, and graphene were optimized. The geometry optimization was performed until the forces acting on the atoms were less than the threshold values depending on the code. See the specific values in the corresponding subsections.

After the optimization of the geometries of H_2, benzene, and graphene, the calculations of H_2 interacting on benzene and graphene were carried out, for each method. In the case of H_2 on benzene, the hydrogen molecule was placed on top of the center of the benzene molecule and perpendicularly oriented with respect to the benzene plane (see Fig. 1). This orientation yields the lowest binding energy of H_2 on benzene. The individual geometries of benzene or graphene and H_2 were kept frozen, with the optimized geometries obtained in the previous step for the corresponding method, and only the distance between the center of mass of H_2 and the benzene or graphene plane was changed. That distance was changed from 2 to 7 Å, for benzene, and from 2 to 6 Å, for graphene, with a step of 0.1 Å. In the case of H_2 on graphene, the hydrogen molecule was placed on top of three sites and with three different orientations of the H_2 axis with respect to the graphene plane.

The approximation of keeping frozen the individual geometries of benzene, graphene, and H_2, and changing only the benzene-H_2 or graphene-H_2 distance, to study the physisorption was checked. Relaxation of all the coordinates of the systems H_2 on benzene and H_2 on graphene, around the minimum of their physisorption energy curves and for a single method, RVV10, was carried out. The minimum is located at a benzene-H_2 distance of 3.1 Å, with H_2 on top of the center of the benzene molecule and perpendicular to the benzene plane, and at a graphene-H_2 distance of 2.96 Å, with H_2 on top of the center of a hexagon and parallel to the benzene plane, for the RVV10 method. This relaxation yielded a geometry with a total energy of about 10^{-4} eV lower than the binding energy obtained by keeping frozen the individual geometries and relaxing only the benzene-H_2 or the graphene-H_2 distance. This difference is very small compared to the binding energy of H_2 on benzene, −0.0450 eV, and on graphene, −0.0629 eV. Therefore, the approximation of keeping frozen the individual geometries is a valid approximation to study the physisorption, taking into account that the physisorption occurs at H_2-surface distances equal or larger than approximately 2.4-2.5 Å. At very short H_2-surface distances, the interaction is strongly repulsive and the approximation will not be valid. Chemisorption effects occur at very short distances and this work is devoted only to physisorption effects.

The interaction energy $E(d)$ between benzene or graphene and a H_2 molecule placed at a distance d from the benzene or graphene plane is defined in terms of the energies of the interacting system and the separated components as
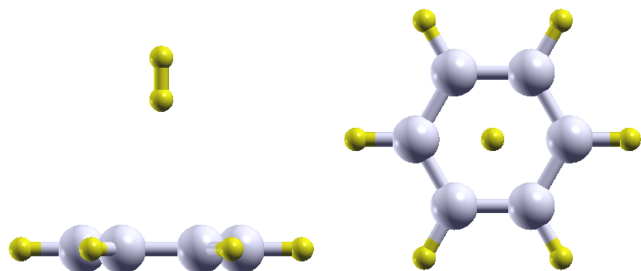
$$E(d) = E(H_2 \text{ on } A; d) - E(H_2) - E(A), \quad (1)$$

where A is benzene or graphene. The binding energy E_b is the interaction energy at the equilibrium H_2-benzene or H_2-graphene plane distance d_e, i.e., $E_b = E(d_e)$. A negative value of E_b means that the molecule is bonded to the benzene molecule or to graphene.

A. Gaussian 09

The Gaussian 09 (G09) code[70] was used to make calculations of H_2 on benzene, but not on graphene. Several methods implemented in the G09 package have been used in the present work: CCSD(T),[24] MP2,[25] PBE,[65,66] VWN,[67] PW91,[68] B97D,[41,69] and PBE-D2.[41] The VWN method uses the LDA for exchange and correlation effects with the Vosko-Wilk-Nusair (VWN) parameterization.[67] PBE and PW91 use GGA functionals due to Perdew, Burke, and Ernzerhof,[65,66] and to Perdew and Wang,[68] respectively. PBE-D2 and B97D include dispersion corrections according to the DFT-D scheme. PBE-D2 stands for the PBE functional and the Grimme's D2 dispersion corrections.[41] B97D is a functional proposed by Grimme,[41] based on the B97 functional of Becke[69] and Grimme's D2 dispersion corrections. It is a reparameterization of the original B97 functional.

This code performs all-electron calculations using Gaussian basis sets to expand the wavefunctions. The basis set used for all the methods is the augmented correlation-consistent basis set, aug-cc-pVTZ, of Dunning et al.[76–80] Basis sets of the aug-cc-pVXZ family contain diffuse functions which are necessary to account for dispersion interactions. The spin restricted calculations (because H_2 and benzene are closed-shell systems) were done self-consistently with a total energy convergence tolerance of 2.72×10^{-5} eV. The optimizations of the geometries were run until the forces on the atoms were lower than 4.63×10^{-3} eV/Å and the displacements of atoms were lower than 1.9×10^{-4} Å.

Dispersion energies are small. For this reason, the interaction energies have been calculated always using the counterpoise correction method of Boys and Bernardi[81] in order to correct the basis set superposition error (BSSE). This has been done for all the methods used with the G09 code.

A test of the basis set is provided in Fig. 2, where a comparison of CCSD(T) calculations of H_2 interacting with benzene, done with the aug-cc-pVDZ, aug-cc-pVTZ, and aug-cc-pVQZ basis sets, is presented. The counterpoise method was used to calculate the interaction energies in Fig. 2. The aug-cc-pVQZ basis set is the largest one. The difference between the aug-cc-pVTZ and aug-cc-pVQZ interaction energies is smaller than 10^{-3} eV/molecule in the region near the minimum, and it becomes negligible at larger H_2-benzene distances. The CCSD(T) interaction energies obtained with the aug-cc-pVQZ basis set are very similar to those obtained using the aug-cc-pVTZ basis set (see Fig. 2), but the computational cost was much higher. Therefore, we selected the aug-cc-pVTZ basis set and the counterpoise method to make the G09 calculations with all the methods.

The use of aug-cc-pVTZ basis sets, the correction of the BSSE, and the value of the self-consistent threshold used
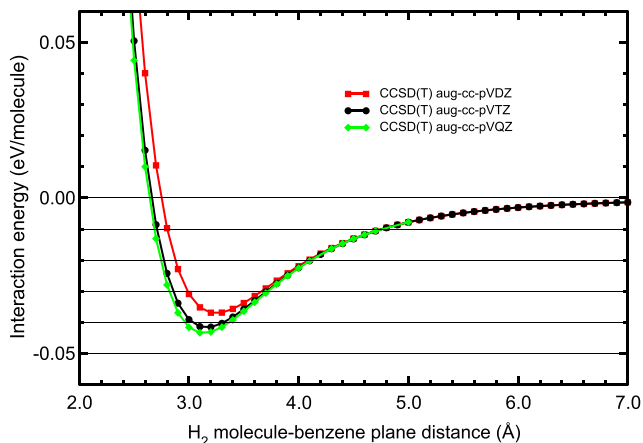

FIG. 1. Lateral and top views of the H_2 molecule on top of the benzene molecule and perpendicular to the benzene-plane.

FIG. 2. Interaction energy between H_2 and benzene as a function of the H_2-benzene distance, obtained by the CCSD(T) method and the counterpoise method, as implemented in the Gaussian 09 code. Calculations performed with the aug-cc-pVDZ, aug-cc-pVTZ, and aug-cc-pVQZ basis sets are compared.

mean that the present G09 calculations have a high degree of precision.

CCSD(T) calculations of H_2 parallel to the benzene plane, using the aug-cc-pVTZ basis set and the counterpoise method, yielded a less negative binding energy, −0.0288 eV, than the CCSD(T) calculations of H_2 perpendicular to the benzene plane in the same conditions, −0.0415 eV. H_2 perpendicular is more stable than H_2 parallel, and therefore, we have chosen the H_2 perpendicular orientation to make the calculations with all the methods.

B. BigDFT

The BigDFT code[71–73] was used to perform PBE+DCACP calculations of H_2 on benzene and graphene. This code[71–73] replaces the core electrons by pseudopotentials and expands the electronic wavefunctions in a basis set of wavelets. The code includes only DFT-based methods. The calculations were done self-consistently with a convergence tolerance of 2.72 $\times 10^{-6}$ eV. Spin-restricted calculations have been carried out. The parameters taken to select the basis wavelets were as follows: a grid spacing of 0.15 bohr for benzene and 0.25 bohr for graphene in the three spatial directions and the values of 9.5 and 9.0 for the coarse and fine grid radius multipliers, respectively. These multipliers are the factors multiplying the coarse and fine radius around each atom. These values were chosen after carrying out tests of the convergence of the interaction energy with respect to the values of the parameters. With these values of the parameters of the basis wavelets, the interaction energies $E(d)$ have a precision of 10^{-4} eV. DCACPs developed by Rothlisberger and co-workers[42–45] were used with the PBE functional. These calculations are called PBE+DCACP throughout the paper.

The geometries of the hydrogen molecule, benzene, and graphene were considered optimized when the forces on the atoms were less than 2×10^{-3} eV/Å. Calculations of H_2 and benzene were done in free boundary conditions. The unit cell for the graphene periodic calculations was a planar layer of 32 carbon atoms and a lattice parameter of 20 Å in the direction perpendicular to the graphene plane. The lattice parameter

of 20 Å was chosen after carrying out tests of the convergence of the interaction energy with respect to the lattice parameter.

C. Quantum Espresso

The Quantum Espresso code was used to make calculations of H_2 physisorbed on benzene with the functionals PBE-TS,[47] PBE-XDM,[48,49] vdW-DF,[30] optB88-vdW,[32] optB86b-vdW,[33] vdW-DF-cx,[34] vdW-DF-C09,[35] vdW-DF2,[36] vdW-DF2-C09,[37] rev-vdW-DF2,[38] and RVV10,[40] and to make calculations of H_2 physisorbed on graphene with the functionals PBE,[65,66] PBE-D2,[41] PBE-TS, PBE-XDM, vdW-DF, optB88-vdW, optB86b-vdW, vdW-DF-cx, vdW-DF-C09, vdW-DF2, vdW-DF2-C09, rev-vdW-DF2, and RVV10. The works of Thonhauser *et al.* and Román-Pérez and Soler are relevant in the practical implementation of the vdW-DF functionals.[82,83] This code uses planewaves basis sets. The kinetic energy cutoff for the wavefunctions was set at 120 Ry and the kinetic energy cutoff for charge density and potential was set at 480 Ry, after carrying out tests of the convergence of the interaction energy with respect to the cutoffs. With these values of the cutoffs, the precision of the interaction energies $E(d)$ is 10^{-4} eV. All the calculations were performed using the Martins-Troullier norm-conserving pseudopotentials,[84] except the PBE-XDM calculations, which were performed using the Kresse-Joubert Projector Augmented-Wave, PAW, pseudopotentials.[85] Only the Γ point was used in the calculations of both benzene and graphene.

The unit cell for the benzene calculations was a cubic supercell with a lattice parameter of 15 Å. The unit cell for the graphene calculations was a hexagonal planar layer of 72

TABLE I. Equilibrium H–H distance in H_2, C–C, and C–H distances in benzene and C–C distance in graphene, in Å, obtained with different methods.

Method	d_{H-H}	d_{C-C} benzene	d_{C-H} benzene	d_{C-C} graphene
CCSD(T)	0.7430	1.3980	1.0839	...
MP2	0.7374	1.3942	1.0822	...
VWN	0.7660	1.3858	1.0937	...
PW91	0.7494	1.3959	1.0890	...
PBE	0.7509	1.3974	1.0909	1.4196
PBE+DCACP	0.7505	1.3973	1.0909	1.4284
B97D	0.7449	1.3988	1.0873	...
PBE-D2	0.7509	1.3982	1.0910	1.4195
PBE-TS	0.7424	1.3917	1.0852	1.4180
PBE-XDM	0.7505	1.3963	1.0905	1.4243
vdW-DF	0.7313	1.3909	1.0797	1.4197
vdW-DF-C09	0.7456	1.3906	1.0884	1.4180
vdW-DF-cx	0.7444	1.3908	1.0879	1.4181
optB86b-vdW	0.7421	1.3906	1.0863	1.4183
optB88-vdW	0.7372	1.3895	1.0825	1.4178
vdW-DF2	0.7276	1.3927	1.0772	1.4224
rev-vdW-DF2	0.7425	1.3910	1.0864	1.4186
vdW-DF2-C09	0.7450	1.3912	1.0882	1.4185
RVV10	0.7363	1.3935	1.0825	1.4218
Reference	0.7414[86]	1.3902[87]	1.0862[87]	1.42[88]

carbon atoms, with a lattice parameter of 15 Å in the direction perpendicular to the graphene plane. The lattice parameter of 15 Å for benzene and graphene was chosen after carrying out tests of the convergence of the interaction energy with respect to the lattice parameter. The SCF procedure was considered converged if the absolute total energy change was below 1.36×10^{-6} eV for benzene calculations and 1.36×10^{-7} eV for graphene calculations. The geometries were considered converged when the forces on the atoms were less than 2.57×10^{-4} eV/Å.

The results of the optimization of the geometries of H_2, benzene, and graphene carried out with the CCSD(T) and MP2 methods and with different functionals are reported in Table I. The theoretical or experimental references for the geometries are at the bottom of that table. The equilibrium H–H distance in the H_2 molecule is 0.7414 Å according to high precision Hylleraas variational calculations.[86] Experimental values of the geometry of benzene, $d_{C-C} = 1.3902 \pm 0.0002$ Å and $d_{C-H} = 1.0862 \pm 0.0015$ Å, were obtained from the work of Plíva et al.[87] The experimental carbon-carbon distance is 1.42 Å in graphite.[88]

III. CALCULATIONS OF H2 PHYSISORBED ON BENZENE: MP2 AND DFT-BASED METHODS VS CCSD(T) METHOD

The interaction energy curves obtained in the calculations are plotted in Figs. 3–5. Some horizontal lines corresponding to 0, −0.01, −0.02, −0.03, −0.04, and −0.05 eV have been plotted in those figures, to guide the eye in the comparison of the different curves. The H_2-benzene plane equilibrium distances and the binding energies obtained with the different methods are given in Table II.

The CCSD(T) results (binding energy, equilibrium H_2-plane distance, and interaction energy curve) are the benchmark and the results obtained with the other methods will be compared with the CCSD(T) results. To make these comparisons possible, the CCSD(T) interaction energy curve is plotted in the three figures of the interaction energy curves: Figures 3–5. The CCSD(T) method yields a binding energy $E_b = -0.0415$ eV and an equilibrium distance $d_e = 3.2$ Å.

The binding energies and the equilibrium distances are features of a single point of the interaction energy curve: its minimum. However, to study the physisorption and the hydrogen storage, two regions in the interaction energy curve must be considered and not only the single point of the minimum: The region around the minimum of the curve, approximately between $d_i = 2.8$ and 4.0 Å, and the tail region of the curve, above $d_i = 4.0$ Å, where d_i is the H_2-benzene surface distance.

The interaction energy curves in Figs. 3–5 can be compared visually with the interaction energy curve obtained in CCSD(T) calculations. That visual comparison is qualitative and in some cases is not accurate. In order to compare quantitatively and more accurately the curves, we have defined the $RMSE_m$, the root-mean-square error, and the $RMSPE_m$, the root-mean-square percentage error, of the region around the minimum of the interaction energy curve, obtained with method F, as

TABLE II. Equilibrium H_2-benzene plane distances, d_e, in Å, and binding energies, E_b, in eV, for H_2 perpendicular to the benzene molecule obtained with different methods. $RMSE_m$ and $RMSE_t$ are in eV, and $RMSPE_m$ and $RMSPE_t$ are in % (see text for their meaning).

Method	d_e	E_b	$RMSE_m$	$RMSPE_m$	$RMSE_t$	$RMSPE_t$
CCSD(T)	3.2	−0.0415	0.0000	0	0.0000	0
MP2	3.1	−0.0487	0.0064	21	0.0006	7
VWN	2.8	−0.0996	0.0365	118	0.0015	35
PW91	3.4	−0.0290	0.0136	43	0.0012	27
PBE	3.4	−0.0204	0.0212	66	0.0030	37
PBE+DCACP	3.3	−0.0413	0.0036	13	0.0011	33
B97D	3.1	−0.0371	0.0035	9	0.0010	12
PBE-D2	3.0	−0.0565	0.0132	44	0.0007	8
PBE-TS	3.2	−0.0561	0.0100	28	0.0014	13
PBE-XDM	3.2	−0.0538	0.0111	34	0.0032	60
vdW-DF	3.5	−0.0450	0.0168	61	0.0073	87
vdW-DF-C09	3.3	−0.0379	0.0058	20	0.0055	83
vdW-DF-cx	3.6	−0.0405	0.0130	46	0.0066	82
optB86b-vdW	3.3	−0.0413	0.0066	24	0.0049	72
optB88-vdW	3.3	−0.0390	0.0055	19	0.0029	52
vdW-DF2	3.3	−0.0448	0.0063	22	0.0013	11
rev-vdW-DF2	3.3	−0.0359	0.0073	24	0.0007	7
vdW-DF2-C09	3.7	−0.0168	0.0275	84	0.0013	11
RVV10	3.1	−0.0450	0.0029	9	0.0004	12

$$ RMSE_m = \sqrt{\sum_{i=1}^{N} \frac{\left(E(d_i)_F - E(d_i)_{CCSD(T)}\right)^2}{N}}, \qquad (2) $$

$$ RMSPE_m = 100 \sqrt{\sum_{i=1}^{N} \frac{\left(E(d_i)_F - E(d_i)_{CCSD(T)}\right)^2}{\left(E(d_i)_{CCSD(T)}\right)^2 N}}, \qquad (3) $$

where d_i runs from $d_1 = 2.8$ Å to $d_N = 4.0$ Å, with a step of 0.01 Å, and $E(d_i)_F$ and $E(d_i)_{CCSD(T)}$ are the interaction energies of H_2 on benzene, for a H_2-benzene surface distance of d_i, obtained with the methods F and CCSD(T), respectively. $RMSE_m$ has the same units as $E(d_i)$, eV, and $RMSPE_m$ is in %. We have also defined the $RMSE_t$ and $RMSPE_t$ quantities as the root-mean-square error and root-mean-square percentage error, respectively, of the tail region of the interaction energy curve. $RMSE_t$ and $RMSPE_t$ are also defined according to Eqs. (2) and (3), respectively, but replacing m by t and d_i running from $d_1 = 4.1$ Å to $d_N = 7.0$ Å, with a step of 0.01 Å.

$RMSE$ is a measure of the similarity between the interaction energy curve obtained with a particular method and the CCSD(T) interaction energy curve. The smaller the value of $RMSE$, the closer the similarity between the two curves. $RMSE_x$ can be also considered as the average difference between the interaction energies of the F and CCSD(T) methods in the region around the minimum (x = m) or in the tail region (x = t). The calculated values of $RMSE_m$, $RMSPE_m$, $RMSE_t$, and $RMSPE_t$ are given in Table II.

The methods studied have been separated into three groups. The first group is composed by the MP2 method and by DFT-based methods that do not include the dispersion interactions. In this group are the VWN, PW91, and PBE methods. Figure 3 contains the interaction energy curves of the first
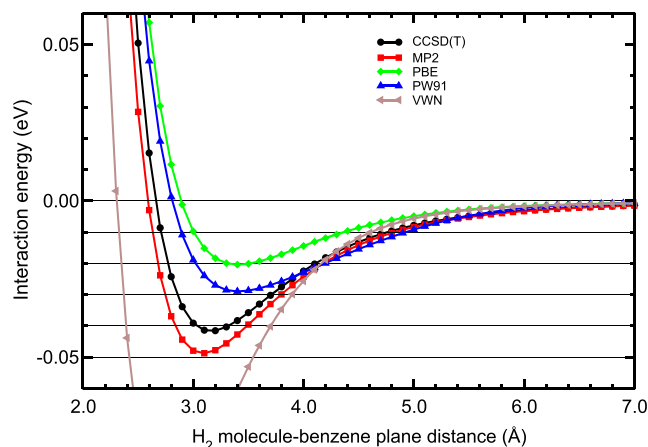
FIG. 3. Interaction energy between H_2 and benzene as a function of the H_2-benzene plane distance, obtained in CCSD(T), MP2, and DFT (VWN, PW91, and PBE) calculations.

group. The second group is composed by DFT-based methods that include the dispersion interactions empirically or semiempirically at different levels of complexity. In this group are the PBE-D2, B97D, PBE-TS, PBE-XDM, and PBE+DCACP methods. The interaction energy curves of the second group are plotted in Fig. 4. The third group is composed by DFT-based methods that include dispersion interactions through non-local correlation functionals that do not depend on external parameters: the family of vdW-DF methods (vdW-DF, optB88-vdW, optB86b-vdW, vdW-DF-cx, and vdW-DF-C09), the family of vdW-DF2 methods (vdW-DF2, vdW-DF2-C09, and rev-vdW-DF2), and the RVV10 method. Their corresponding energy curves are plotted in Fig. 5. In Subsections III A–III D, we compare the interaction energy curves of the methods studied with the CCSD(T) interaction energy curve of H_2 on benzene.

A. MP2 and DFT methods that do not include dispersion interactions vs CCSD(T)

First, we compare the MP2, VWN, PW91, and PBE results. The VWN, PW91, and PBE functionals do not include dispersion interactions. The VWN functional overestimates the H_2-benzene interaction, resulting in a larger binding energy
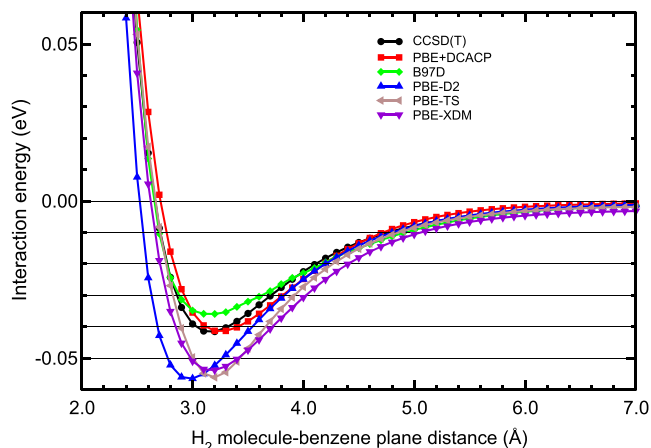

FIG. 4. Interaction energy between H_2 and benzene as a function of the H_2-benzene plane distance, obtained in CCSD(T) and DFT-D (PBE+DCACP, B97D, PBE-D2, PBE-TS, PBE-XDM) calculations.
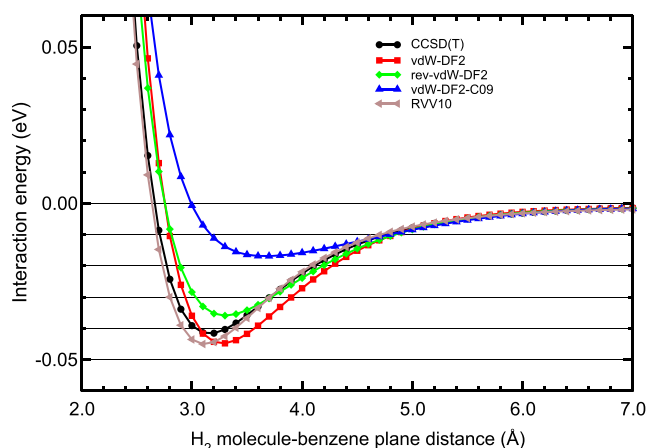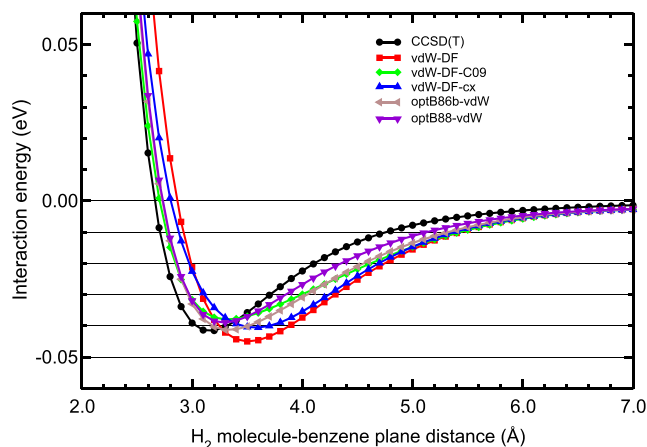

FIG. 5. Interaction energy between H_2 and benzene as a function of the H_2-benzene plane distance, obtained in CCSD(T) calculations and using the non-local functionals: The vdW-DF family, the vdW-DF2 family, and RVV10.

and a shorter equilibrium distance compare to the benchmark. The VWN binding energy is −0.0996 eV, 2.4 times larger than the CCSD(T) binding energy. The VWN equilibrium distance is 2.8 Å, while the CCSD(T) equilibrium distance is 3.2 Å. The GGA functionals, PBE and PW91, underestimate the H_2-benzene interaction, resulting in smaller binding energies and larger equilibrium distances. These two functionals yield the binding energies of −0.0204 and −0.0290 eV, respectively, and a common equilibrium distance of 3.4 Å. Those features of the VWN, PW91, and PBE functionals are general and well known for other systems. The quantity $RMSE_m$ measures all the differences between the curves. The values of $RMSE_m$ of VWN, PW91, and PBE are very large, 0.0426, 0.0151, and 0.0227 eV, respectively, indicating a large dissimilarity between these curves and the CCSD(T) curve. MP2 yields a binding energy of −0.0487 eV, slightly larger than the CCSD(T) binding energy, an equilibrium distance of 3.1 Å, and a value of $RMSE_m$ equal to 0.0074 eV, much smaller than the values of $RMSE_m$ of the VWN, PW91, and PBE methods.

B. DFT methods that include dispersion interactions empirically or semiempirically vs CCSD(T)

Second, we analyze the empirical and semiempirical DFT methods (PBE+DCACP, B97D, PBE-D2, PBE-TS, and PBE-XDM). The introduction of dispersion in the empirical and

semiempirical DFT methods has a clear effect on improving the interaction energy curve between H_2 and benzene, yielding better binding energies and equilibrium distances than the LDA and GGA methods. The binding energies of the DFT-D methods (B97D, PBE-D2, PBE-TS, and PBE-XDM) are within 11%-36% of the CCSD(T) binding energy. These results are consistent with several previous results on van der Waals clusters[41,44,57,89–93] showing that DFT-D methods deliver binding energies within 10%-30% of those of the benchmark methods (CCSD(T) and MP2).

If we compare the interaction energy curves of the DFT-D methods with the CCSD(T) interaction energy curve (see Fig. 4 and Table II), we find that B97D yields an interaction energy curve close to the CCSD(T) energy curve, with a small value of $RMSE_m$, 0.0035 eV, while the PBE-D2, PBE-TS, and PBE-XDM interaction energy curves are far from the CCSD(T) curve, with larger values of $RMSE_m$: 0.0132, 0.0100, and 0.0111 eV, respectively. The large dissimilarity between the interaction energy curves of PBE-D2, PBE-TS, and PBE-XDM, and the CCSD(T) curve, can be better noticed in the large values of their $RMSPE_m$: 44%, 28%, and 34%, respectively.

The DFT+DCACP method includes dispersion corrections through the dispersion corrected atom-centered pseudopotentials, DCACPs. The effect of those corrections can be obtained by making a comparison between PBE and PBE+DCACP calculations of the interaction energy curve of H_2 with benzene in Figs. 3 and 4. The difference in the binding energy, between PBE and PBE+DCACP, is about 0.02 eV, and the difference in the equilibrium distance is 0.1 Å. On the other hand, the PBE+DCACP binding energy is very close to the CCSD(T) binding energy: The difference in the binding energy is very small, 2×10^{-4} eV. Even more important than the binding energy is the fact that the PBE+DCACP and the CCSD(T) interaction energy curves are in very good agreement, as can be seen in Fig. 4 and also in the small value of $RMSE_m$ of the PBE+DCACP method, 0.0036 eV (see Table II).

C. DFT methods that include dispersion interactions through non-local functionals vs CCSD(T)

Third, the non-local functionals are analyzed: vdW-DF, vdW-DF-C09, vdW-DF-cx, optB86b-vdW, optB88-vdW, vdW-DF2, rev-vdW-DF2, vdW-DF2-C09, and RVV10. The functionals of the vdW-DF and vdW-DF2 families, except the vdW-DF2-C09 functional, yield binding energies very close to the CCSD(T) binding energy: between 0% and 10% above or below the CCSD(T) binding energy (see Table II). However, the equilibrium H_2-benzene plane distance of some of these functionals is far from the CCSD(T) equilibrium H_2-benzene plane distance. On the other hand, RVV10 yields an equilibrium distance of 3.1 Å and a binding energy of −0.0450 eV, very close to the CCSD(T) equilibrium distance and binding energy, 3.2 Å and −0.0415 eV, respectively.

The interaction energy curves obtained with the non-local functionals are plotted in Fig. 5. The binding energies of the functionals of the vdW-DF family are very close to the CCSD(T) binding energy. Their interaction energy curves are similar to the CCSD(T) interaction energy curve in the region

around the minimum. However, they are very different from the CCSD(T) interaction energy curve in the tail region, as can be seen in Fig. 5 and especially in their values of $RMSPE_t$ in Table II. The values of $RMSPE_t$ of the vdW-DF family are very large: They range from 52% to 87%, which means that in the tail region the interaction energy curves of this family are very different from the CCSD(T) curve.

As regards to the vdW-DF2 family, the interaction energy curves of the vdW-DF2 and rev-vdW-DF2 methods are close to the CCSD(T) interaction energy curve in both regions. Notice the low values of $RMSPE_t$ of these two methods in Table II: 11% and 7%, respectively. The interaction energy curve of vdW-DF2-C09 is very far from the CCSD(T) curve in the region around the minimum. Finally, the RVV10 curve is also close to the CCSD(T) curve in both regions, especially in the region around the minimum of the curve. Its values of $RMSE_m$ and $RMSPE_m$ are low: 0.0029 eV and 9%, respectively.

D. DFT methods that best compare with CCSD(T) results of H_2 on benzene

From the plots of the interaction energy curves in Figs. 4 and 5 and the values of $RMSE_m$, $RMSPE_m$, $RMSE_t$, and $RMSPE_t$ in Table II, it can be concluded that, among the DFT methods studied, the RVV10, B97D, and PBE+DCACP interaction energy curves of H_2 on benzene are the most similar to the CCSD(T) interaction energy curve. The agreement between the RVV10, B97D, and PBE+DCACP curves, and the CCSD(T) curve is remarkable, considering that the values of the interaction energy are very low. The values of $RMSE_m$ of the RVV10, B97D, and PBE+DCACP methods are small: 0.0029, 0.0035, and 0.0036 eV, respectively. The B97D and
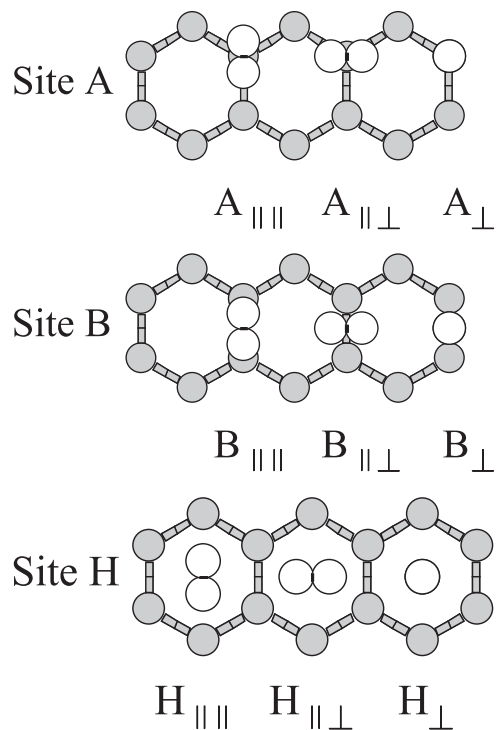

FIG. 6. The nine configurations of the H_2 molecule on top of the graphene surface. Three sites: on carbon Atom, A, on carbon-carbon Bond, B, and on the center of the Hexagon, H. For each site, three different orientations of the molecular axis are explored.

PBE+DCACP methods were built by fitting the parameters of these methods to data sets of high level *ab initio* calculations of weakly bonded systems[41,45] that do not include H_2-benzene. According to the present results, B97D and PBE+DCACP also yield results very similar to the CCSD(T) results for H_2 on benzene.

IV. CALCULATIONS OF H_2 PHYSISORBED ON GRAPHENE: DFT-BASED METHODS VS EXPERIMENTAL DATA

Calculations of H_2 physisorbed on graphene, on different sites and with different orientations of the molecular axis of H_2 with respect to the graphene plane, have been carried out. PBE and different DFT-based methods that include dispersion interactions have been used. The molecule was placed on top of the three different sites of graphene: the center of a hexagon, H, the center of a C–C bond, B, and a carbon atom, A. The three main orientations of the molecular axis of the H_2 molecule have been studied: the axis perpendicular to the graphene plane, $\perp$, the axis parallel to the graphene plane and parallel to two C–C bonds of the hexagon, $\parallel\parallel$, and the axis parallel to the graphene plane and perpendicular to two C–C bonds of the hexagon, $\parallel \perp$. The combination of site and orientation is a configuration. We have studied the nine configurations of H_2 on graphene plotted in Fig. 6. The following notation has been used for the configurations: The letter indicates the site where the molecule was placed and the set of

TABLE III. Equilibrium H_2-graphene plane distances, d_e, in Å, and binding energies, E_b, in eV, for H_2 on different sites on graphene and with different orientations of the molecular axis, obtained with the PBE, PBE+DCACP, PBE-D2, PBE-TS, PBE-XDM, methods, and the family of vdW-DF methods.

Configuration	PBE d_e	PBE E_b	PBE+DCACP d_e	PBE+DCACP E_b	PBE-D2 d_e	PBE-D2 E_b	PBE-TS d_e	PBE-TS E_b	PBE-XDM d_e	PBE-XDM E_b
$A_{\parallel\parallel}$	3.6	−0.0093	3.3	−0.0396	3.1	−0.0489	3.1	−0.0624	3.2	−0.0486
$A_{\parallel\perp}$	3.6	−0.0093	3.3	−0.0399	3.1	−0.0489	3.1	−0.0624	3.2	−0.0486
$A_{\perp}$	3.6	−0.0111	3.3	−0.0428	3.1	−0.0577	3.2	−0.0633	3.2	−0.0513
$B_{\parallel\parallel}$	3.6	−0.0095	3.2	−0.0405	3.0	−0.0503	3.1	−0.0637	3.2	−0.0496
$B_{\parallel\perp}$	3.5	−0.0111	3.3	−0.0396	3.1	−0.0491	3.1	−0.0630	3.2	−0.0489
$B_{\perp}$	3.5	−0.0111	3.3	−0.0431	3.1	−0.0582	3.2	−0.0634	3.2	−0.0515
$H_{\parallel\parallel}$	3.5	−0.0110	3.1	−0.0478	2.9	−0.0608	2.9	−0.0750	3.0	−0.0567
$H_{\parallel\perp}$	3.5	−0.0110	3.1	−0.0473	2.9	−0.0608	2.9	−0.0750	3.0	−0.0567
$H_{\perp}$	3.5	−0.0116	3.2	−0.0459	2.9	−0.0641	3.1	−0.0688	3.1	−0.0543

Configuration	vdW-DF d_e	vdW-DF E_b	vdW-DF-C09 d_e	vdW-DF-C09 E_b	vdW-DF-cx d_e	vdW-DF-cx E_b	optB86b-vdW d_e	optB86b-vdW E_b	optB88-vdW d_e	optB88-vdW E_b
$A_{\parallel\parallel}$	3.3	−0.0761	3.2	−0.0683	3.3	−0.0708	3.2	−0.0719	3.2	−0.0686
$A_{\parallel\perp}$	3.3	−0.0761	3.2	−0.0683	3.3	−0.0708	3.2	−0.0719	3.2	−0.0686
$A_{\perp}$	3.4	−0.0748	3.2	−0.0691	3.4	−0.0693	3.2	−0.0721	3.2	−0.0698
$B_{\parallel\parallel}$	3.3	−0.0769	3.2	−0.0692	3.3	−0.0714	3.2	−0.0728	3.2	−0.0696
$B_{\parallel\perp}$	3.3	−0.0762	3.2	−0.0684	3.3	−0.0709	3.2	−0.0720	3.2	−0.0687
$B_{\perp}$	3.4	−0.0748	3.2	−0.0693	3.4	−0.0694	3.2	−0.0724	3.2	−0.0700
$H_{\parallel\parallel}$	3.2	−0.0798	3.1	−0.0744	3.3	−0.0744	3.1	−0.0780	3.1	−0.0752
$H_{\parallel\perp}$	3.2	−0.0798	3.1	−0.0744	3.3	−0.0744	3.1	−0.0780	3.1	−0.0752
$H_{\perp}$	3.3	−0.0754	3.1	−0.0711	3.4	−0.0703	3.2	−0.0742	3.1	−0.0716

TABLE IV. Equilibrium H_2-graphene plane distances, d_e, in Å, and binding energies, E_b, in eV, for H_2 on different sites on graphene and with different orientations of the molecular axis, obtained with the family of vdW-DF2 methods and the RVV10 method.

Configuration	vdW-DF2 d_e	vdW-DF2 E_b	rev-vdW-DF2 d_e	rev-vdW-DF2 E_b	vdW-DF2-C09 d_e	vdW-DF2-C09 E_b	RVV10 d_e	RVV10 E_b
$A_{\parallel\parallel}$	3.2	−0.0611	3.2	−0.0511	3.4	−0.0298	3.1	−0.0532
$A_{\parallel\perp}$	3.2	−0.0611	3.3	−0.0525	3.4	−0.0298	3.1	−0.0532
$A_{\perp}$	3.2	−0.0633	3.2	−0.0527	3.4	−0.0306	3.1	−0.0577
$B_{\parallel\parallel}$	3.2	−0.0623	3.2	−0.0521	3.4	−0.0303	3.1	−0.0546
$B_{\parallel\perp}$	3.2	−0.0611	3.2	−0.0511	3.4	−0.0298	3.1	−0.0534
$B_{\perp}$	3.2	−0.0634	3.2	−0.0529	3.4	−0.0306	3.1	−0.0580
$H_{\parallel\parallel}$	3.1	−0.0681	3.1	−0.0575	3.3	−0.0326	3.0	−0.0627
$H_{\parallel\perp}$	3.1	−0.0681	3.1	−0.0575	3.3	−0.0326	3.0	−0.0627
$H_{\perp}$	3.2	−0.0646	3.2	−0.0548	3.4	−0.0311	3.1	−0.0611

symbols after the letter denotes the orientation of the molecular axis.

The binding energies of H_2 on graphene and the equilibrium H_2-graphene surface distances obtained with different DFT methods for the nine configurations of H_2 on graphene are shown in Tables III and IV. The site with the lowest binding energies for all the DFT methods studied in Tables III and IV is the center of the hexagon, site H. The binding energies of H_2 on the C–C bond, site B, and on the carbon atom, site A, are less negative. The lowest binding energy in Tables III and IV, for most of the DFT methods studied, corresponds to the $H_{\parallel\parallel}$
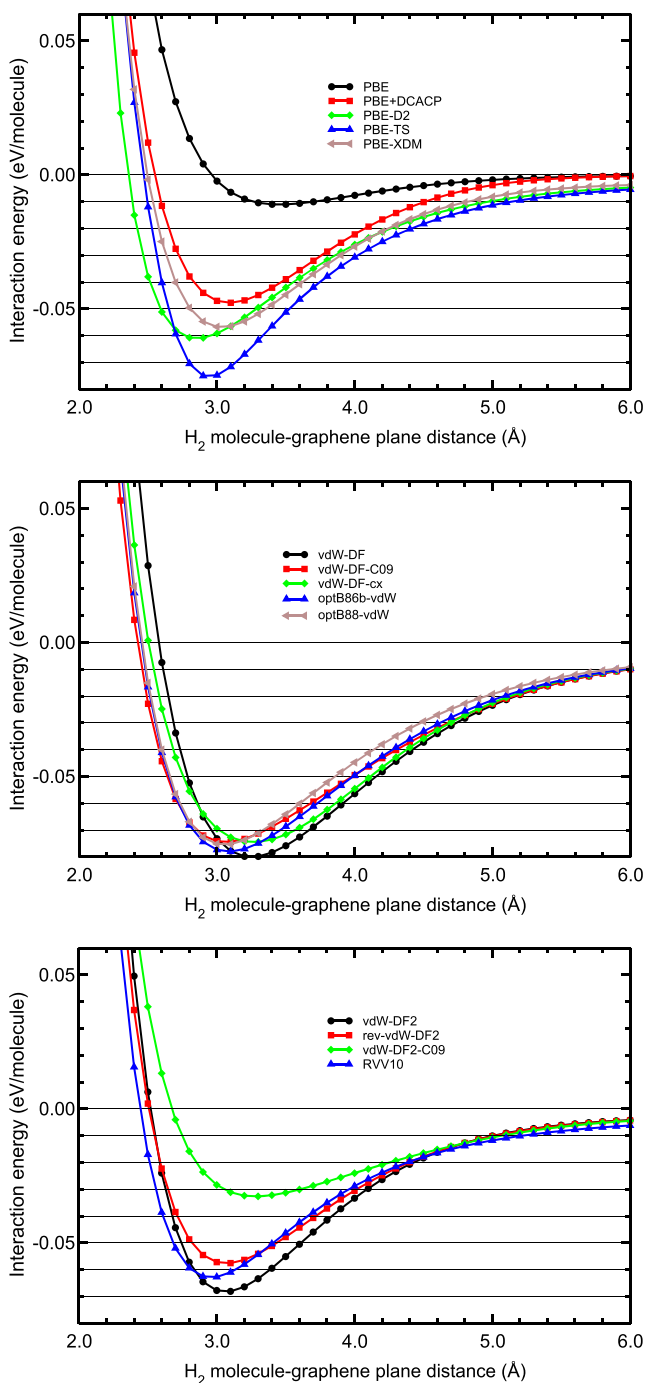

FIG. 7. Interaction energy between H_2 and graphene as a function of the H_2-graphene plane distance, obtained with PBE and with different DFT-based methods that include dispersion interactions. H_2 is in the configuration $H_{\parallel\parallel}$.

configuration. Nevertheless, the other two orientations of the molecule on site H have binding energies close to the $H_{\parallel\parallel}$ configuration. Since the $H_{\parallel\parallel}$ configuration has the lowest binding energies, the interaction energy curves have been calculated only for the $H_{\parallel\parallel}$ configuration and are plotted in Fig. 7.

The theoretical results should be compared with experiments. Mattera et al.[64] measured the energy of the lowest level of H_2 physisorbed on graphite. They reported a value of −0.041 61 eV, with an experimental accuracy of 0.000 25 eV. Costanzo et al.[52] used a model[94] to discount the effect of the other graphene layers of graphite, in order to obtain the experimental energy of the lowest level of H_2 physisorbed on graphene. They found that the energy should be corrected by 6×10^{-3} eV. The adsorption energy obtained by Mattera et al.[64] on graphite, −0.0416 eV, turned out to be −0.0476 eV on graphene, according to that model. This is the experimental value of the adsorption energy of the lowest level of H_2 physisorbed on graphene, $E_{ads,exp}$.

To obtain the adsorption energy of the lowest level of H_2 physisorbed on graphene, E_{ads}, we have to calculate the zero point energy of the interaction energy curve, E_{zp}, and subtract it from the binding energy, i.e., $E_{ads} = E_b - E_{zp}$. We have calculated the zero point energy E_{zp} of the interaction energy curve obtained with every DFT-based method, for the $H_{\parallel\parallel}$ configuration and later, the adsorption energy of the lowest level of H_2 physisorbed on graphene, $E_{ads} = E_b - E_{zp}$.

The results of the calculations of H_2 on graphene for the $H_{\parallel\parallel}$ configuration are shown in Table V. To calculate accurately the zero point energy, we have done more calculations for H_2-graphene distances d around the minimum, with a step of 0.01 Å. Therefore the results in Table V are slightly different from the results of the configuration $H_{\parallel\parallel}$ in Tables III and IV.

The theoretical value of the adsorption energy of the lowest level of H_2 on graphene, E_{ads}, is also compared with the experimental value, $E_{ads,exp}$, in that table. The adsorption energy of the lowest level obtained with the PBE-D2,

TABLE V. Equilibrium H_2-graphene plane distances, d_e, in Å, binding energies, E_b, in eV, and adsorption energies of the lowest level, E_{ads}, for H_2 on configuration $H_{\parallel\parallel}$, obtained with different DFT methods. Error = $E_{ads} - E_{ads,exp}$ is in eV and Relative error = 100 Error/$|E_{ads,exp}|$ is in %.

Method	d_e	E_b	E_{ads}	Error	Relative error
PBE	3.46	−0.0110	−0.0062	0.0414	87.0
PBE+DCACP	3.06	−0.0478	−0.0382	0.0094	19.7
PBE-D2	2.85	−0.0610	−0.0507	−0.0031	−6.5
PBE-TS	2.94	−0.0754	−0.0610	−0.0134	−28.2
PBE-XDM	3.05	−0.0568	−0.0470	0.0006	1.3
vdW-DF	3.24	−0.0800	−0.0706	−0.0230	−48.3
vdW-DF-C09	3.06	−0.0745	−0.0657	−0.0181	−38.0
vdW-DF-cx	3.26	−0.0745	−0.0666	−0.0190	−39.9
optB86b-vdW	3.08	−0.0780	−0.0686	−0.0210	−44.1
optB88-vdW	3.06	−0.0754	−0.0656	−0.0180	−37.8
vdW-DF2	3.06	−0.0682	−0.0573	−0.0097	−20.4
rev-vdW-DF2	3.07	−0.0576	−0.0481	−0.0005	−1.1
vdW-DF2-C09	3.28	−0.0326	−0.0266	0.0210	44.1
RVV10	2.96	−0.0629	−0.0520	−0.0044	−9.2

PBE-XDM, rev-vdW-DF2, and RVV10 methods is close to the experimental value: within 5×10^{-3} eV and 10% of the experimental value, $E_{ads,exp} = -0.0476$ eV. The adsorption energies obtained with the other DFT methods are less accurate.

V. SUMMARY AND CONCLUSIONS

The goal of this work has been to search for DFT-based methods that reproduce accurately the physisorption interaction between H_2 and benzene and also between H_2 and graphene, in particular, DFT-based methods that reproduce the CCSD(T) interaction energy curve of H_2 on benzene and the experimental data of the physisorption of H_2 on graphene. To reach this goal, calculations of the interaction energy curves of H_2 on benzene using the CCSD(T), MP2, PBE, VWN, PW91, PBE+DCACP, B97D, PBE-D2, PBE-TS, PBE-XDM, vdW-DF, vdW-DF-C09, vdW-DF-cx, ptB86b-vdW, optB88-vdW, vdW-DF2, rev-vdW-DF2, vdW-DF2-C09, and RVV10 methods, and calculations of the interaction energy curves of H_2 on graphene using the PBE, PBE+DCACP, PBE-D2, PBE-TS, PBE-XDM, vdW-DF, vdW-DF-C09, vdW-DF-cx, optB86b-vdW, optB88-vdW, vdW-DF2, rev-vdW-DF2, vdW-DF2-C09, and RVV10 methods, have been carried out.

The most relevant conclusions are as follows: (a) The B97D, RVV10, and PBE+DCACP methods yield interaction energy curves of H_2-benzene that reproduce rather well the CCSD(T) interaction energy curve: within 4×10^{-3} eV and 13%, on average, of the CCSD(T) interaction energy curve in the region around the minimum (see Figs. 4 and 5, and Table II). Therefore, these three DFT-based methods provide a good description of the physisorption of H_2 on benzene, with a good compromise between accuracy and computer cost. (b) The rev-vdW-DF2, PBE-XDM, PBE-D2, and RVV10 methods yield adsorption energies of the lowest level of H_2 on graphene very close to the experimental result: within 5×10^{-3} eV and 10% of the experimental value, -0.0476 eV. Hence, these DFT methods can be used to obtain a good description of the physisorption of H_2 on graphene, with a good compromise between accuracy and computer cost. Among all the DFT methods studied in the present work, RVV10 is the method giving the most accurate physisorption results in both, benzene and graphene. These conclusions are of particular interest for the investigation of hydrogen storage on porous carbon materials.

ACKNOWLEDGMENTS

[1] P. Bernard and R. Chahine, Langmuir **17**, 1950 (2001).
[2] Y. Gogotsi, A. Nikitin, H. Ye, W. Zhou, J. E. Fischer, B. Yi, H. C. Foley, and M. W. Barsoum, Nat. Mater. **2**, 591 (2003).
[3] S. Challet, P. Azaïs, R. J.-M. Pellenq, O. Isnard, J.-L. Soubeyroux, and L. Duclaux, J. Phys. Chem. Solids **65**, 541 (2004).
[4] Y. Gogotsi, R. K. Dash, G. Yushin, T. Yildirim, G. Laudisio, and J. E. Fischer, J. Am. Chem. Soc. **127**, 16006 (2005).
[5] G. Yushin, R. Dash, J. Jagiello, J. E. Fischer, and Y. Gogotsi, Adv. Funct. Mater. **16**, 2288 (2006).
[6] M. Jordá-Beneyto, F. Suárez-García, D. Lozano-Castelló, D. Cazorla-Amorós, and A. Linares-Solano, Carbon **45**, 293 (2007).
[7] M. Jordá-Beneyto, D. Lozano-Castelló, F. Suárez-García, D. Cazorla-Amorós, and A. Linares-Solano, Microporous Mesoporous Mater. **112**, 235 (2008).
[8] Y. Gogotsi, C. Portet, S. Osswald, J. M. Simmons, T. Yildirim, G. Laudisio, and J. E. Fischer, Int. J. Hydrogen Energy **34**, 6314 (2009).
[9] F. Suárez-García, E. Vilaplana-Ortego, M. Kunowsky, M. Kimura, A. Oya, and A. Linares-Solano, Int. J. Hydrogen Energy **34**, 9141 (2009).
[10] I. Cabria, M. J. López, and J. A. Alonso, in *Handbook of Nanophysics: Functional Nanomaterials*, edited by K. D. Sattler (CRC Press, Boca Raton, 2010), Chap. 41, pp. 41-1–41-16.
[11] M. Kunowsky, J. P. Marco-Lozar, A. Oya, and A. Linares-Solano, Carbon **50**, 1407 (2012).
[12] G. G. I. Wróbel-Iwaniec and N. Díez, Int. J. Hydrogen Energy **40**, 5788 (2015).
[13] G. Sethia and A. Sayari, Carbon **99**, 289 (2016).
[14] M. Rzepka, P. Lamp, and M. A. de la Casa-Lillo, J. Phys. Chem. B **102**, 10894 (1998).
[15] Q. Wang and J. K. Johnson, Mol. Phys. **95**, 299 (1998).
[16] Q. Wang and J. K. Johnson, J. Chem. Phys. **110**, 577 (1999).
[17] S. Patchkovskii, J. S. Tse, S. N. Yurchenko, L. Zhechkov, T. Heine, and G. Seifert, Proc. Natl. Acad. Sci. U. S. A. **102**, 10439 (2005).
[18] I. Cabria, M. J. López, and J. A. Alonso, Carbon **45**, 2649 (2007).
[19] G. Mpourmpakis and G. E. Froudakis, J. Nanosci. Nanotechnol. **8**, 3091 (2008).
[20] I. Cabria, M. J. López, and J. A. Alonso, J. Chem. Phys. **128**, 144704 (2008).
[21] I. Cabria, M. J. López, and J. A. Alonso, Phys. Rev. B **78**, 075415 (2008).
[22] Y. Ihm, V. R. Cooper, L. Peng, and J. R. Morris, J. Phys.: Condens. Matter **24**, 424205 (2012).
[23] J. A. Alonso, I. Cabria, and M. J. López, J. Mater. Res. **28**, 589 (2013).
[24] J. Čížek, J. Chem. Phys. **45**, 4256 (1966).
[25] C. Møller and M. S. Plesset, Phys. Rev. **46**, 618 (1934).
[26] K. E. Riley, M. Pitoňák, P. Jurečka, and P. Hobza, Chem. Rev. **110**, 5023 (2010).
[27] K. E. Riley and P. Hobza, Wiley Interdiscip. Rev.: Comput. Mol. Sci. **1**, 3 (2011).
[28] P. Hobza, Acc. Chem. Res. **45**, 663 (2012).
[29] J. Klimeš and A. Michaelides, J. Chem. Phys. **137**, 120901 (2012).
[30] M. Dion, H. Rydberg, E. Schröder, D. C. Langreth, and B. I. Lundqvist, Phys. Rev. Lett. **92**, 246401 (2004).
[31] P. Hyldgaard, K. Berland, and E. Schröder, Phys. Rev. B **90**, 075148 (2014).
[32] J. Klimeš, D. R. Bowler, and A. Michaelides, J. Phys.: Condens. Matter **22**, 022201 (2010).
[33] J. Klimeš, D. R. Bowler, and A. Michaelides, Phys. Rev. B **83**, 195131 (2011).
[34] K. Berland and P. Hyldgaard, Phys. Rev. B **89**, 035412 (2014).
[35] V. R. Cooper, Phys. Rev. B **81**, 161104(R) (2010).
[36] K. Lee, E. D. Murray, L. Kong, B. I. Lundqvist, and D. C. Langreth, Phys. Rev. B **82**, 081101(R) (2010).
[37] I. Hamada and M. Otani, Phys. Rev. B **82**, 153412 (2010).
[38] I. Hamada, Phys. Rev. B **89**, 121103(R) (2014).
[39] O. A. Vydrov and T. van Voorhis, J. Chem. Phys. **133**, 244103 (2010).
[40] R. Sabatini, T. Gorni, and S. de Gironcoli, Phys. Rev. B **87**, 041108(R) (2013).
[41] S. Grimme, J. Comput. Chem. **27**, 1787 (2006).
[42] O. A. von Lilienfeld, I. Tavernelli, U. Rothlisberger, and D. Sebastiani, Phys. Rev. Lett. **93**, 153004 (2004).
[43] O. A. von Lilienfeld, I. Tavernelli, U. Rothlisberger, and D. Sebastiani, Phys. Rev. B **71**, 195119 (2005).
[44] E. Tapavicza, I. C. Lin, O. A. von Lilienfeld, I. Tavernelli, M. D. Coutinho-Neto, and U. Rothlisberger, J. Chem. Theory Comput. **3**, 1673 (2007).
[45] I. Lin, M. D. Coutinho-Neto, C. Felsenheimer, O. A. von Lilienfeld, I. Tavernelli, and U. Rothlisberger, Phys. Rev. B **75**, 205131 (2007).
[46] See http://lcbc.epfl.ch/page-71135-en.html for Library of Dispersion-Corrected Atom-Centered Potentials (accessed May 11, 2017).
[47] A. Tkatchenko and M. Scheffler, Phys. Rev. Lett. **102**, 073005 (2009).
[48] A. D. Becke and E. R. Johnson, J. Chem. Phys. **127**, 154108 (2007).
[49] A. O. de la Roza and E. R. Johnson, J. Chem. Phys. **136**, 174109 (2012).
[50] P. L. Silvestrelli, Phys. Rev. Lett. **100**, 053002 (2008).

[51]P. L. Silvestrelli, J. Phys. Chem. A **113**, 5224 (2009).

[52]F. Costanzo, P. L. Silvestrelli, and F. Ancilotto, J. Chem. Theory Comput. **8**, 1288 (2012).

[53]A. Ambrosetti and P. L. Silvestrelli, Phys. Rev. B **85**, 073101 (2012).

[54]P. L. Silvestrelli and A. Ambrosetti, J. Chem. Phys. **140**, 124107 (2014).

[55]Y. Zhao and D. G. Truhlar, J. Chem. Theory Comput. **1**, 415 (2005).

[56]Q. Hill and C.-K. Skylaris, Proc. R. Soc. A **465**, 669 (2009).

[57]C. D. Sherrill, T. Takatani, and E. G. Hohenstein, J. Phys. Chem. A **113**, 10146 (2009).

[58]Y. Liu and W. A. Goddard III, J. Phys. Chem. Lett. **1**, 2550 (2010).

[59]K. S. Thanthiriwatte, E. G. Hohenstein, L. A. Burns, and C. D. Sherrill, J. Chem. Theory Comput. **7**, 88 (2011).

[60]J. C. Flick, D. Kosenkov, E. G. Hohenstein, C. D. Sherrill, and L. V. Slipchenko, J. Chem. Theory Comput. **8**, 2835 (2012).

[61]M. Doemer, I. Tavernelli, and U. Rothlisberger, J. Chem. Theory Comput. **9**, 955 (2013).

[62]M. Callsen and I. Hamada, Phys. Rev. B **91**, 195103 (2015).

[63]I. Cabria, M. J. López, and J. A. Alonso, Int. J. Hydrogen Energy **36**, 10748 (2011).

[64]L. Mattera, R. Rosatelli, C. Salvo, F. Tommasini, U. Valbusa, and G. Vidali, Surf. Sci. **93**, 515 (1980).

[65]J. P. Perdew, K. Burke, and M. Ernzerhof, Phys. Rev. Lett. **77**, 3865 (1996).

[66]J. P. Perdew, K. Burke, and M. Ernzerhof, Phys. Rev. Lett. **78**, 1396 (1997).

[67]S. H. Vosko, L. Wilk, and M. Nusair, Can. J. Phys. **58**, 1200 (1980).

[68]J. P. Perdew and Y. Wang, Phys. Rev. B **45**, 13244 (1992).

[69]A. D. Becke, J. Chem. Phys. **107**, 8554 (1997).

[70]M. J. Frisch, G. W. Trucks, H. B. Schlegel, G. E. Scuseria, M. A. Robb, J. R. Cheeseman, G. Scalmani, V. Barone, B. Mennucci, G. A. Petersson *et al.*, GAUSSIAN 09, Revision B.01, Gaussian, Inc., Wallingford, CT, 2009.

[71]L. Genovese, A. Neelov, S. Goedecker, T. Deutsch, S. A. Ghasemi, A. Willand, D. Caliste, O. Zilberberg, M. Rayson, A. Bergman *et al.*, J. Chem. Phys. **129**, 014109 (2008).

[72]T. Deutsch and L. Genovese, Collect. SFN **12**, 33 (2011).

[73]See http://bigdft.org for BigDFT Code (accessed May 11, 2017).

[74]See http://www.quantum-espresso.org for Quantum Espresso Code (accessed May 11, 2017).

[75]P. Giannozzi, S. Baroni, N. Bonini, M. Calandra, R. Car, C. Cavazzoni, D. Ceresoli, G. L. Chiarotti, M. Cococcioni, I. Dabo *et al.*, J. Phys.: Condens. Matter **21**, 395502 (2009).

[76]T. H. Dunning, Jr., J. Chem. Phys. **90**, 1007 (1989).

[77]R. A. Kendall, T. H. Dunning, Jr., and R. J. Harrison, J. Chem. Phys. **96**, 6796 (1992).

[78]D. E. Woon and T. H. Dunning, Jr., J. Chem. Phys. **98**, 1358 (1993).

[79]K. A. Peterson, D. E. Woon, and T. H. Dunning, Jr., J. Chem. Phys. **100**, 7410 (1994).

[80]E. R. Davidson, Chem. Phys. Lett. **260**, 514 (1996).

[81]S. F. Boys and F. Bernardi, Mol. Phys. **19**, 553 (1970).

[82]T. Thonhauser, V. R. Cooper, S. Li, A. Puzder, P. Hyldgaard, and D. C. Langreth, Phys. Rev. B **76**, 125112 (2007).

[83]G. Román-Pérez and J. M. Soler, Phys. Rev. Lett. **103**, 096102 (2009).

[84]M. Troullier and J. L. Martins, Phys. Rev. B **43**, 1993 (1991).

[85]G. Kresse and J. Joubert, Phys. Rev. B **59**, 1758 (1999).

[86]J. S. Sims and S. A. Hagstrom, J. Chem. Phys. **124**, 094101 (2006).

[87]J. Plíva, J. W. C. Johns, and L. Goodman, J. Mol. Spectrosc. **148**, 427 (1991).

[88]R. W. G. Wyckoff, *Crystal Structures* (Interscience, New York, 1963), Vol. 1.

[89]P. Jurečka, J. Cerny, P. Hobza, and D. R. Salahub, J. Comput. Chem. **28**, 555 (2007).

[90]M. Kabeláč, H. Valdés, E. C. Sherer, C. J. Cramer, and P. Hobza, Phys. Chem. Chem. Phys. **9**, 5000 (2007).

[91]C. Morgado, J. McNamara, I. Hillier, N. Burton, and M. Vincent, J. Chem. Theory Comput. **3**, 1656 (2007).

[92]K. E. Riley, J. Vondrášek, and P. Hobza, Phys. Chem. Chem. Phys. **9**, 5555 (2007).

[93]A. Vázquez-Mayagoitia, C. D. Sherrill, E. Aprà, and B. G. Sumpter, J. Chem. Theory Comput. **6**, 727 (2010).

[94]A. D. Crowell and J. S. Brown, Surf. Sci. **123**, 296 (1982).